

Nanoscale

Accepted Manuscript



This is an *Accepted Manuscript*, which has been through the Royal Society of Chemistry peer review process and has been accepted for publication.

Accepted Manuscripts are published online shortly after acceptance, before technical editing, formatting and proof reading. Using this free service, authors can make their results available to the community, in citable form, before we publish the edited article. We will replace this *Accepted Manuscript* with the edited and formatted *Advance Article* as soon as it is available.

You can find more information about *Accepted Manuscripts* in the [Information for Authors](#).

Please note that technical editing may introduce minor changes to the text and/or graphics, which may alter content. The journal's standard [Terms & Conditions](#) and the [Ethical guidelines](#) still apply. In no event shall the Royal Society of Chemistry be held responsible for any errors or omissions in this *Accepted Manuscript* or any consequences arising from the use of any information it contains.



Cite this: DOI: 10.1039/xxxxxxxxxx

Charge transfer at carbon nanotube-graphene van der Waals heterojunctions

Yuanda Liu,^{a‡} Fengqiu Wang,^{a‡*} Yujie Liu,^a Xizhang Wang,^b Yongbing Xu,^{a*} Rong Zhang^{a*}

Received Date

Accepted Date

DOI: 10.1039/xxxxxxxxxx

www.rsc.org/journalname

Carbon nanotubes and graphene are two most widely investigated low-dimensional materials for photonic and optoelectronic devices. Combining these two materials into all-carbon hybrid nanostructures has shown enhanced properties in a range of devices, such as photodetectors and flexible electrodes. Interfacial charge transfer is the most fundamental physical process that directly impacts device design and performance, but remains a subject less well studied. Here, we complemented Raman spectroscopy with photocurrent probing, a robust way of illustrating the interfacial built-in fields, and unambiguously revealed both the static and dynamic (photo-induced) charge transfer processes at the nanotube-graphene interfaces. Significantly, the effects of nanotube species, i.e. metallic as opposed to semiconducting, is for the first time compared. Of all the devices examined, graphene sheet was found p-type doped by (6,5) chirality-enriched semiconducting SWNTs (s-SWNTs), while n-type doped by highly pure (>99%) metallic SWNTs (m-SWNTs). Our results provide important design guidelines for all-carbon hybrid based devices.

Low-dimensional carbon allotropes, including one-dimensional carbon nanotubes (CNTs) and two-dimensional graphene, exhibit properties that are suitable for a wide range of optoelectronic applications such as photodetectors, light-emitting devices, and transparent electrodes^{1–5}. These two materials share the same sp² hybridization of carbon atoms,⁶ and can be merged into hybrid systems either covalently⁷ or by van der Waals (vdW) interactions^{8–10}. The hybrid system displays enhanced mechanical strength while retaining excellent optical and electrical prop-

erties, and is envisioned to offer optimized performance than the individual constituent materials.¹¹ For example, it is recently demonstrated that high responsivities, fast and broadband photo-detection can be achieved in a phototransistor based on a vdW bonded film consisting of single-wall carbon nanotubes (SWNTs) and graphene.¹⁰ The formation of nanometer-scale one-dimensional vdW heterojunctions which can be harnessed in an optoelectronic device is asking for refined knowledge of the fundamental charge behavior at the nanotube-graphene interface, an important topic that remains less investigated.

To date, only a few previous reports were dedicated to the study of electrostatic charge transfer at the nanotube-graphene heterojunctions,^{12–14} typically via detecting characteristic peak shifts in Raman spectroscopy. Paulus *et al.* observed an electron transfer of $1.12 \times 10^{13} \text{ cm}^{-2}$ from an individual metallic SWNT to graphene, suggesting the presence of a relatively small potential offset between metallic SWNT and graphene¹². Rao *et al.* synthesized SWNT bundles directly on graphene by chemical vapor deposition (CVD), but found that graphene donates electrons to the SWNT bundles¹³. It has been difficult to interpret and reconcile these seemingly contradictory results, and establish a generalized physical picture about the charge transfer scenario at the SWNT-graphene heterojunctions. In addition, both works analysed only the Raman spectra, the role photogenerated carriers may have played, an important aspect of the charge behavior at the interface, was not taken into consideration. Therefore, it is highly desirable to combine Raman spectroscopy with other examination tools to obtain deeper insights into the charge transfer dynamics at SWNT-graphene vdW heterojunctions.

Here, we address the limitations of previous studies by complementing Raman spectroscopy performed on atomically thin SWNT-graphene hybrid films, with associated photocurrent measurements. To this end, photoresponse of a phototransistors based on the hybrid film is corroborated with the characteristic peak shifts as obtained in Raman spectroscopy, providing essential information about the built-in electric fields and the Fermi

^aSchool of Electronic Science and Engineering and Collaborative Innovation Center of Advanced Microstructures, Nanjing University, Nanjing 210093, China. E-mail: fwang@nju.edu.cn; ybxu@nju.edu.cn; rzhang@nju.edu.cn

^bSchool of Chemistry and Chemical Engineering, Nanjing University, Nanjing 210093, China.

‡ These authors contributed equally to this work.

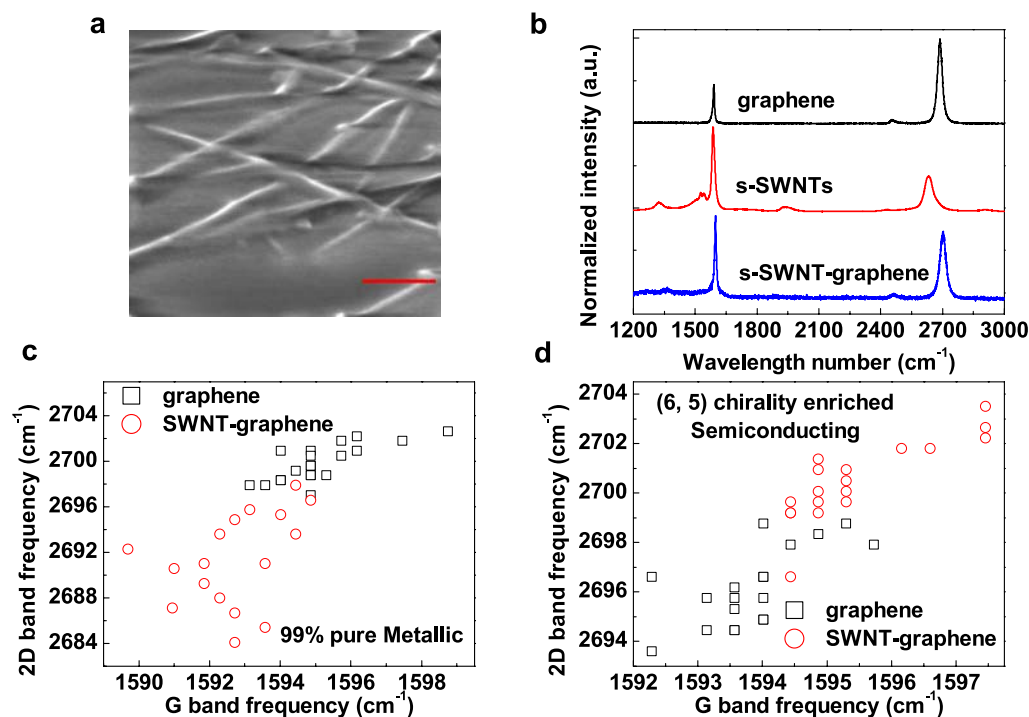


Fig. 1 a, SEM micrograph of SWNTs on SiO₂/Si substrate. Scale bar, 100 nm. b, Raman spectroscopic characterization of graphene, SWNTs and SWNT-graphene hybrid, respectively. The laser power was kept at 1 mW to avoid the heating effect. c, d, Peak positions of G and 2D Raman bands of graphene before and after contact made by 99% pure metallic and (6, 5) chirality enriched (>93%) semiconducting SWNTs, respectively.

level information about the hybrid system. The robustness of this approach have for the first time enabled straightforward assignment of the electrostatic doping conditions at the SWNT-graphene interfaces. Our results unambiguously confirmed p-type (n-type) doping of graphene upon semiconducting (metallic) SWNTs-graphene contact under dark conditions, and indicate that it will be possible to construct nanometer scale p-n junction based on conduction-type modulation in SWNT-graphene hybrid system.

The SWNT-graphene hybrid film is fabricated by transferring CVD-grown graphene onto spin-coated SWNTs layer, and the SWNTs layer were spincoated from the NMP (N-methyl-2-pyrrolidone) solution on the SiO₂ (285 nm)/Si substrate, as detailed in Ref. 10. We characterized the carbon nanotubes on SiO₂/Si substrates with a FEI field emission SEM (SEM, Scanning Electron Microscopy), as shown in Figure 1a. Most of the nanotubes appear straight and formed an atomically thin carbon nanotubes network on SiO₂/Si substrate. Meanwhile, due to the use of highly purified nanotubes, no metal catalyst particles are present, greatly mitigating charge effects from extrinsic factors.

Raman spectroscopy is widely used for characterizing electronic and structural properties of carbon materials and allows the determination of doping level, intrinsic stress, and layer number of graphene. Raman spectra in this work were measured in the backscattering configuration. The scattered light was analyzed on a Horiba Jobin Yvon LabRAM HR 800 system using a 514 nm excitation laser operating at 1 mW, 100X objective lens with about $\sim 1 \mu\text{m}$ beam spot diameter, and 1800 lines/mm grat-

ing with about 0.45 cm^{-1} spectral resolution. No polarization analyzer was used, so that light polarized both perpendicular and parallel to the scattering plane was collected. We first investigated the case where graphene is contacted by (6, 5) chirality enriched (>93%) semiconducting s-SWNTs (Sigma-Aldrich). Figure 1b shows the Raman spectrum of graphene, s-SWNT layer and s-SWNT/graphene hybrid, respectively. The black curve in Figure 1b is a typical Raman spectrum of graphene with three featured peaks: D, G ($\sim 1589.7 \text{ cm}^{-1}$), and 2D ($\sim 2687.2 \text{ cm}^{-1}$) peak. The D peak is due to the breathing modes of sp^2 rings and requires a defect for its activation.¹⁵ The absence of the D peak indicates defect-free nature of the graphene sample. The 2D peak can be well fitted by a symmetric and sharp Lorentzian peak with FWHM (Full Width at Half Maximum) $\sim 26.2 \text{ cm}^{-1}$, signature of single layer graphene. Also evident from the spectrum of graphene is an I_{2D}/I_G ratio of ~ 2.2 together with the area ratio $A_{2D}/A_G \sim 6.6$, indicative of monolayer graphene with reasonably good quality. The characteristic Raman modes of SWNTs¹⁶ are the RBM (radial breathing mode) ($100\text{-}300 \text{ cm}^{-1}$), the G band ($1500\text{-}1700 \text{ cm}^{-1}$), the D band ($1300\text{-}1400 \text{ cm}^{-1}$) and the 2D band ($2600\text{-}2700 \text{ cm}^{-1}$). Due to the curvature of the SWNTs, the G peak splits into two components G^- (at $\sim 1542 \text{ cm}^{-1}$) and G^+ (at $\sim 1586 \text{ cm}^{-1}$). For SWNT/graphene hybrid material, Raman features of graphene arising from the interfacial charge transfer under dark conditions include the shift of G and 2D band positions, a slight increase in the D peak, and a depression of I_{2D}/I_G ratio.

A comparison of the G and 2D band positions of graphene before and after contacted by SWNTs is summarized, as shown

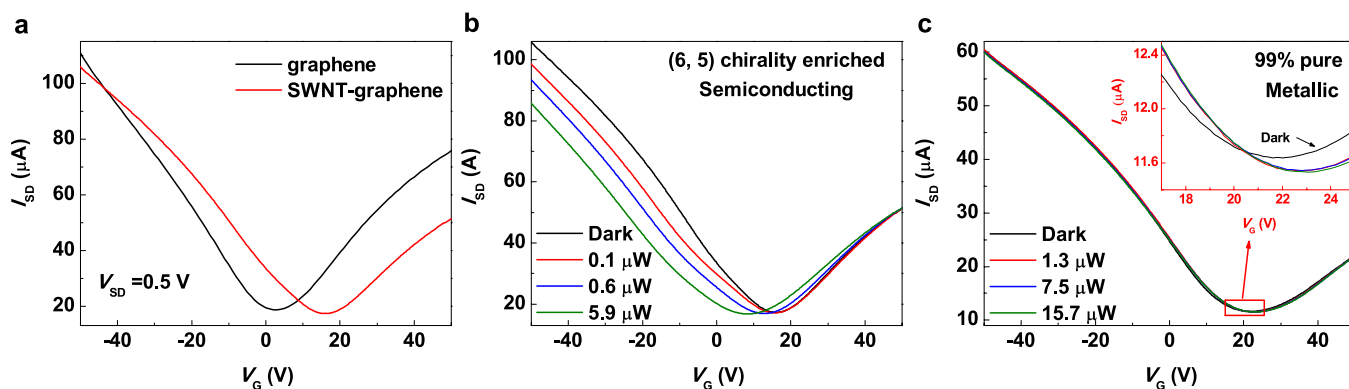


Fig. 2 a, Transfer characteristics of graphene, s-SWNT-graphene phototransistor under dark conditions. It is shown that the Dirac point shifts to the right after s-SWNTs functionalization. $V_{SD}=0.5$ V. b, source-drain current characteristics of s-SWNT-graphene phototransistor as a function of back gate voltage under light excitation. Excitation wavelength is 650 nm. Increasing the illumination power leads to a photogating effect that shifts the Dirac point to the left, indicating that photogenerated electrons transfer from s-SWNTs to graphene sheet, resulting in n-type photodoping of graphene sheet. c, Source-drain current characteristics of metallic SWNT-graphene phototransistor as a function of back gate voltage under light excitation. The inset shows the enlarged view of the section highlighted by the red rectangle. For metallic SWNTs, it is found that the transfer curve shifts toward positive V_G with increasing the illumination power and the Dirac point shifts to the right. These observations indicate that electrons transfer from graphene sheet to metallic SWNTs, resulting in p-type photodoping of graphene sheet, which is opposite to the effect observed for semiconducting SWNTs based hybrid devices. We attribute the observed phenomenon for metallic SWNTs condition to thermocouple effect. Hot electrons generate in the graphene sheet under light illumination and transfer to metallic SWNTs, resulting in the transfer curve right shifting.

in Figure 1c and Figure 1d. It should be noted that the data points shown correspond to Raman measurements on >15 different spots from each of the three regions: graphene only, SWNT only and SWNT-graphene hybrid regions (all three regions were on the same SiO_2/Si substrate and electrically isolated), in order to obtain generalizable doping information. Upon contacting with 99% pure metallic SWNTs (m-SWNTs, Nanointegris), G and 2D bands of graphene downshift by ~ 2.6 cm^{-1} and ~ 2 cm^{-1} , respectively. This indicates electron doping of the graphene sheet, or in other words, electrons transfer from metallic SWNTs to graphene, as consistent with previous results¹². For semiconducting SWNT-graphene scenario, it is found that both G and 2D peaks of graphene upshifts. Our finding of hole doping in the graphene sheet upon contacting s-SWNTs can be used to qualitatively support the observations made by Rao *et al.*¹², in the case semiconducting tubes constitute the main contribution for charge transfer.

To study the dynamic charge transfer, phototransistors using SWNT-graphene hybrid as the channel are fabricated. The back-gated phototransistor devices are fabricated using standard photolithography, metal deposition by electron beam evaporation and lift-off. The electrical measurements were carried out in a closed cycle cryogenic probe station under vacuum (10^{-6} Torr) at room-temperature and the data were collected by a Keithley-4200 semiconductor parameter analyzer. Figure 2a shows the transfer curves of the graphene and SWNT-graphene transistor measured in the absence of light. Compared with pure graphene channel based transistor, the transfer curve of s-SWNT-graphene transistor becomes asymmetric and the Dirac point (the charge neutrality point) shifts from about 3 V to a positive gate voltage of about 16 V, indicative of p-doping in the graphene sheet by semiconducting SWNTs. Figure 2b illustrates the photoresponse of semiconducting SWNT-graphene phototransistor under 650 nm

laser light illumination. We observed that illumination caused the Dirac point to shift leftward, and thus the source-drain current decreases for $V_{BG} < V_D$ where the carrier transport is hole-dominated, but increases for $V_{BG} > V_D$, where carrier transport is electron-dominated. Photocarrier generation at the graphene layer is negligible due to ultrafast carrier recombination. Figure 2c shows the photocurrent characteristics of metallic SWNT-graphene phototransistor. Different from the s-SWNTs case, it is observed that the transfer curve made a small but discernable shift towards higher gate voltage with increasing 650 nm illumination, indicating that electrons transfer from graphene sheet to metallic SWNTs, resulting in p-type photodoping of graphene sheet. As junctions formed by metallic SWNTs and graphene is of Ohmic contact nature¹⁴, we attribute the photocarrier dynamics to thermocouple effect, *i. e.* hot electrons generate in the graphene sheet under light illumination transfer to metallic SWNTs, resulting in the transfer curve right shifting.

Finally, we provide a qualitative, phenomenological and generalized physical picture underpinning previous^{12–14} and present interfacial charge transfer observations in terms of the shifting of the Fermi level (E_F). When graphene is made to interface with metallic tubes, Fermi levels will be hybridized to an intermediate value. Due to the Ohmic nature of the contact between the two materials, no built-in field is present at the interface. The dominating photocarrier dynamics is hot electrons in graphene transferring to metallic tubes. Our experimental findings support the view that CVD graphene tends to exhibit a lower Fermi level than metallic tubes, among various factors, CVD-grown graphene is known to be slightly p-doped due to substrate oxide¹⁷ (this unintentional p-doping is illustrated in Figure 3a). Subsequently, when semiconducting SWNTs are considered (Figure 3b), they also tend to lower the effective Fermi level of graphene (or m-SWNT-graphene hybrid), but with built-in electric fields estab-

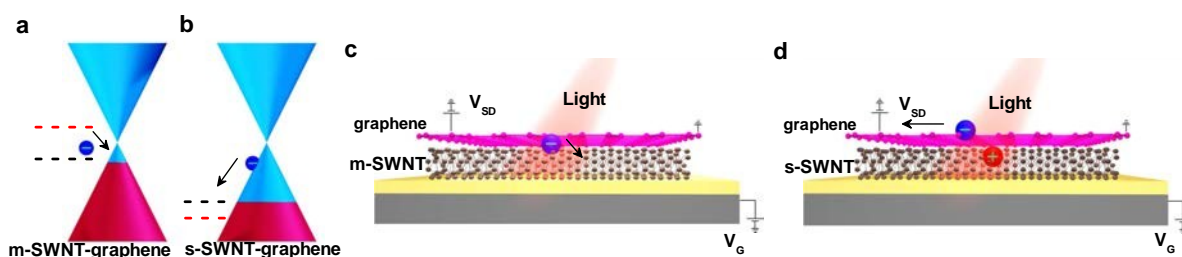


Fig. 3 a, b, Schematic of Fermi level shifting in graphene before and after modification by metallic and semiconducting SWNTs, respectively (under dark condition). Red and black dashed lines schematically denote the Fermi-levels in SWNT for pre-equilibrium and equilibrium conditions, respectively. c, d, Schematic diagram showing the photoexcited carriers transporting process at the interface between graphene and metallic or semiconducting SWNT, respectively. For metallic SWNTs, the photoresponse is governed by hot electrons originating in graphene. While for semiconducting SWNTs, a built-in electric field is established at the heterojunction. Photogenerated electrons in semiconducting SWNT are transferred to graphene under the built-in field, leaving holes trapped in the SWNT.

lished both at the s-SWNT-graphene interface and at the junctions where semiconducting and metallic nanotubes make contact. Upon photoexcitations of semiconducting SWNTs, photo-generated electron-hole pairs would separate under the built-in electric field, resulting in greatly enhanced photocurrent. The conceptual schematic diagrams were proposed to visualize the photoexcited carriers transferring process, as shown in Figure 3c and 3d.

In conclusion, in contrast to the conventional method for studying the electrostatic doping scenario at the carbon nanotube-graphene interface, we for the first time complement Raman spectroscopy with photocurrent probing in SWNT-graphene based phototransistors. We uncover that charge transfer dynamics at SWNT-graphene heterojunctions are chirality-dependent and that a generalized physical picture can be utilized to interpret the interfacial electronic properties in SWNT-graphene hybrid. Our results suggest that it will be possible to develop all-carbon hybrid with controllable electrical and optoelectrical behaviors by engineering nanoscale architectures with customized SWNT chiralities, and provide important design guidelines for novel devices based on this emerging low-dimensional hybrid materials.

This work was supported in part by National Key Basic Research Program of China 2014CB921101, 2011CB301900, 2013CBA01604; National Natural Science Foundation of China 61378025, 61450110087, 61427812, 61274102; Jiangsu Province Shuangchuang Team Program. Y.D.L. acknowledges funding of International Postdoctoral Exchange Fellowship Program 20150023, the China Postdoctoral Science Foundation 2014M551558 and Jiangsu Planned Projects for Postdoctoral Research Funds 1402028B.

References

- 1 A. K. Geim and K. S. Novoselov, *Nat. Mater.* **6**(3), 183 (2007).
- 2 P. Avouris, M. Freitag, and V. Perebeinos, *Nat. Photonics* **2**(6), 341 (2008).
- 3 P. Avouris, Z. Chen, and V. Perebeinos, *Nat. Nanotechnol.* **2**(10), 605 (2007).
- 4 J. Misewich, R. Martel, P. Avouris, J. Tsang, S. Heinze, and J. Tersoff, *Science* **300**(5620), 783 (2003).
- 5 M. Freitag, J. Chen, J. Tersoff, J. C. Tsang, Q. Fu, J. Liu, and P. Avouris, *Phys. Rev. Lett.* **93**(7), 076803 (2004).
- 6 K. S. Novoselov, A. K. Geim, S. V. Morozov, D. Jiang, Y. Zhang, S. V. Dubonos, I. V. Grigorieva, and A. A. Firsov, *Science* **306**(5696), 666 (2004).
- 7 Z. Yan, Z. Peng, G. Casillas, J. Lin, C. Xiang, H. Zhou, Y. Yang, G. Ruan, A. R. O. Raji, and E. L. Samuel, *ACS Nano* **8**(5), 5061 (2014).
- 8 X. Lin, P. Liu, Y. Wei, Q. Li, J. Wang, Y. Wu, C. Feng, L. Zhang, S. Fan, and K. Jiang, *Nat. Commun.* **4** (2013).
- 9 I. N. Kholmanov, C. W. Magnuson, R. Piner, J. Y. Kim, A. E. Aliev, C. Tan, T. Y. Kim, A. A. Zakhidov, G. Sberveglieri, and R. H. Baughman, *Adv. Mater.* **27**(19), 3053 (2015)
- 10 Y. Liu, F. Wang, X. Wang, X. Wang, E. Flahaut, X. Liu, Y. Li, X. Wang, Y. Xu, Y. Shi, and R. Zhang, *Nat. Commun.* **6**, 8589 (2015).
- 11 R. Lv, E. Cruz-Silva, and M. Terrones, *ACS Nano* **8**(5), 4061 (2014).
- 12 G. L. C. Paulus, Q. H. Wang, Z. W. Ulissi, T. P. McNicholas, A. Vijayaraghavan, C. J. Shih, Z. Jin, and M. S. Strano, *Small* **9**(11), 1954 (2013).
- 13 R. Rao, N. Pierce, and A. Dasgupta, *Appl. Phys. Lett.* **105**(7), 073115 (2014).
- 14 T. Pei, H. Xu, Z. Zhang, Z. Wang, Y. Liu, Y. Li, S. Wang, and L. Peng, *Appl. Phys. Lett.* **99**(11), 113102 (2011).
- 15 T. M. G. Mohiuddin, A. Lombardo, R. R. Nair, A. Bonetti, G. Savini, R. Jalil, N. Bonini, D. M. Basko, C. Galiotis, and N. Marzari, *Physical Review B* **79**(20), 205433 (2009).
- 16 A. Kukovecz, C. Kramberger, V. Georgakilas, M. Prato, and H. Kuzmany, *The European Physical Journal B-Condensed Matter and Complex Systems* **28**(2), 223 (2002).
- 17 W-J. Yu, Y. Liu, H. Zhou, A. Yin, Z. Li, Y. Huang, and X. Duan, *Nat. Nanotechnol.* **8**, 952 (2013).